Immunity
Article

Intravital Imaging Reveals Distinct Dynamics for Natural Killer and CD8$^+$ T Cells during Tumor Regression

Jacques Deguine,[1,2,*] Béatrice Breart,[1,2,4] Fabrice Lemaître,[1,2] James P. Di Santo,[3] and Philippe Bousso[1,2,*]
[1]Institut Pasteur, Dynamics of Immune Responses Unit, 75015 Paris, France
[2]INSERM U668, Equipe Avenir, 75015 Paris, France
[3]Institut Pasteur, Innate Immunity Unit; Inserm U668, 75015 Paris, France
[4]Present address: Skirball institute, Molecular Pathogenesis Department, NYU Langone Medical Center, New York, NY 10016, USA
*Correspondence: jacques.deguine@pasteur.fr (J.D.), philippe.bousso@pasteur.fr (P.B.)
DOI 10.1016/j.immuni.2010.09.016

SUMMARY

Recognition of NKG2D ligands by natural killer (NK) cells plays an important role during antitumoral responses. To address how NKG2D engagement affects intratumoral NK cell dynamics, we performed intravital microscopy in a Rae-1β-expressing solid tumor. This NKG2D ligand drove NK cell accumulation, activation, and motility within the tumor. NK cells established mainly dynamic contacts with their targets during tumor regression. In sharp contrast, cytotoxic T lymphocytes (CTLs) formed stable contacts in tumors expressing their cognate antigen. Similar behaviors were observed during effector functions in lymph nodes. In vitro, contacts between NK cells and their targets were cytotoxic but did not elicit sustained calcium influx nor adhesion, whereas CTL contact stability was critically dependent on extracellular calcium entry. Altogether, our results offer mechanistic insight into how NK cells and CTLs can exert cytotoxic activity with remarkably different contact dynamics.

INTRODUCTION

Natural killer (NK) cells are endowed with the ability to directly eliminate transformed or infected cells and are also able to regulate adaptive immune responses through cytokine production (Yokoyama et al., 2004). NK cell recognition of target cells is mediated by a balance between inhibiting and activating signals (Lanier, 2005). NKG2D is a well-characterized activating receptor of the lectin-like family (Burgess et al., 2008) expressed by NK cells, most NKT cells, and subsets of T cells (Raulet, 2003). NKG2D recognizes a variety of ligands distantly related to MHC class I proteins, namely members of the retinoic acid early-inducible-1 (RAE-1) family as well as H60 and MULT1 in mice; MHC class I chain-related proteins (MICA and MICB); and members of the RAET1 family (also called ULBPs) in humans (Nausch and Cerwenka, 2008). These ligands are often overexpressed by tumor cells in both humans (Groh et al., 1999) and mice (Cerwenka et al., 2000; Diefenbach et al., 2000) as a result of the direct effect of oncogenes (Routes et al., 2005) or through chronic activation of the DNA damage response pathway (Gasser et al., 2005). In vivo, ectopic expression of NKG2D ligands induces the rejection of tumor cell lines by NK cells (Cerwenka et al., 2001; Diefenbach et al., 2001) in a perforin-dependent manner (Hayakawa et al., 2002; Smyth et al., 2004). Furthermore, antibody-mediated blockade of the NKG2D pathway has been shown to increase the susceptibility of mice to methylcholanthrene-induced sarcoma (Smyth et al., 2005). In this model, expression of NKG2D ligands was found to be higher when the NK cell response was deficient, implying that NK cells participate in tumor immunoediting (Dunn et al., 2004). Finally, mice deficient for the receptor NKG2D showed an accelerated tumor development in models of spontaneous prostate adenocarcinoma and B cell lymphoma, but not in MCA-induced sarcomas (Guerra et al., 2008). Altogether, these data illustrate the important role of NK cells in the surveillance and elimination of tumors expressing NKG2D ligands. However, a number of important questions remain unanswered. In particular, how NKG2D ligand expression influences NK cell recruitment and trafficking in solid tumors is still unknown. It is also unclear how NK cells interact with targets within the tumor microenvironment.

Using intravital two-photon imaging (Cahalan et al., 2002), we and others have characterized the cellular dynamics of intratumoral cytotoxic T lymphocytes (CTLs) (Boissonnas et al., 2007; Breart et al., 2008; Mrass et al., 2006). In the early phases of tumor regression, CTL velocity was drastically reduced, with many tumor-specific CTLs forming long-lasting contacts with their targets in vivo (Boissonnas et al., 2007; Mrass et al., 2006). Furthermore, tumor cell apoptosis was associated with stable contacts with one or several CTLs (Breart et al., 2008). Likewise, in vitro studies have shown that NK cells form stable contacts with their targets during which lytic granules are secreted at the interface of the effector and the target cell (reviewed in Orange, 2008). However, whether stable interactions also form in vivo has not yet been investigated.

To address these issues, we have combined intravital microscopy and a model of Rae-1β- or, to investigate CTL activity, ovalbumin-, expressing solid tumor (Diefenbach et al., 2001). We show that NKG2D ligand expression promotes NK cell accumulation, motility, and dissemination within the tumor. Surprisingly,

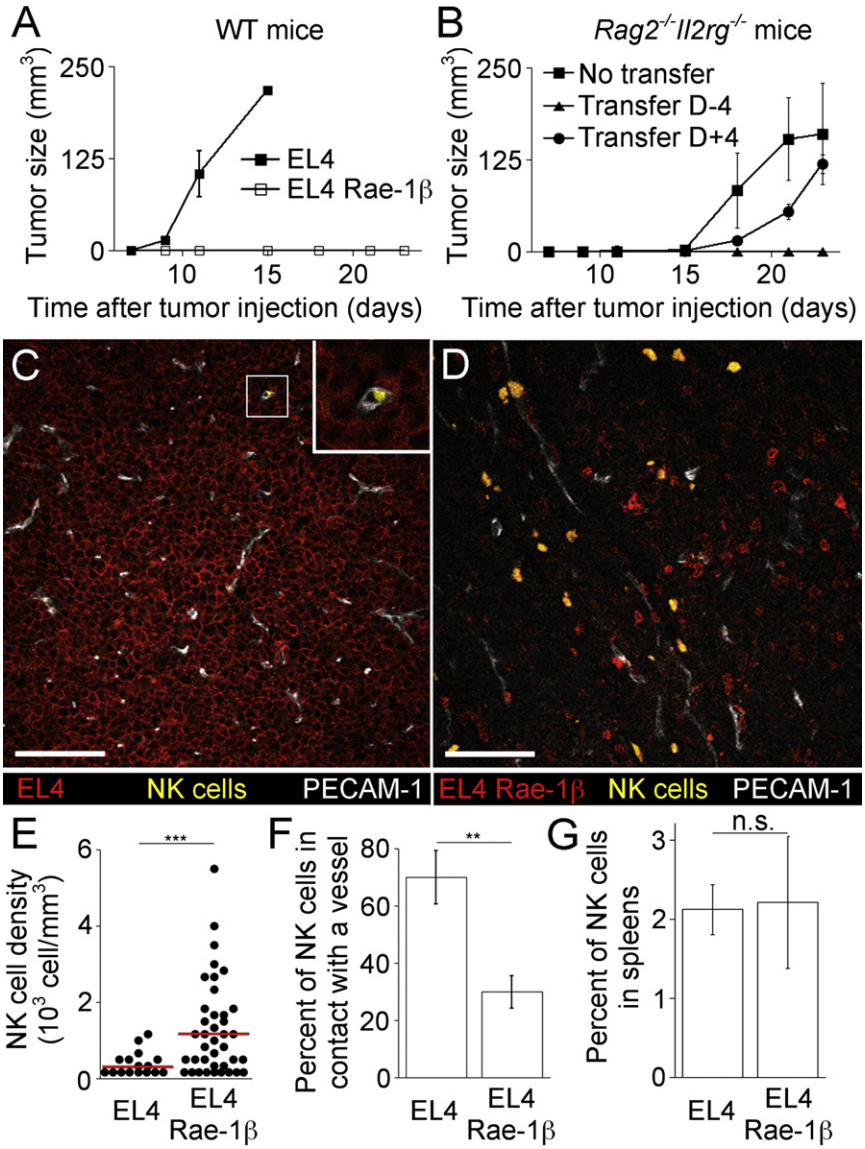

Figure 1. Rae-1β Expression by EL4 Tumor Cells Results in Higher Intratumoral NK Cell Density and Dissemination

(A) Growth of EL4 (filled squares) and EL4 Rae-1β (open squares) tumors in wild-type C57BL/6 mice.

(B) Growth of EL4 Rae-1β tumors in *Rag2*$^{-/-}$*Il2rg*$^{-/-}$ mice in the absence of NK cells (squares) or after NK cell adoptive transfer 4 days before (triangles) or after (circles) tumor injection. Data are presented as mean ± SEM of three mice and are representative of two independent experiments.

(C and D) Four days after tumor injection, GFP-expressing NK cells were transferred in *Rag2*$^{-/-}$*Il2rg*$^{-/-}$ mice. Representative sections of EL4 (C) and EL4 Rae-1β (D) tumors (red) showing infiltration of NK cells (yellow) were analyzed 4 days after NK cell transfer. Blood vessels were stained with anti-PECAM-1 mAb (white). Scale bars represent 100 μm.

(E) NK cell density in EL4 and EL4 Rae-1β tumors. Each dot represents the NK cell density in one 775 × 775 × 10 μm section ($p < 0.001$).

(F) Percentage of NK cells in direct contact with a blood vessel in EL4 and EL4 Rae-1β tumors ($p < 0.01$).

(G) Percentages of NK1.1^{+} cells in the spleens of reconstituted *Rag2*$^{-/-}$*Il2rg*$^{-/-}$ mice bearing an EL4 or an EL4 Rae-1β tumor 4 days after NK cell transfer (n.s., not significant, 3 mice per group). Data are representative of at least two independent experiments. Error bars represent SEM.

NK cells and CTLs exhibited strikingly different intratumoral behavior with most NK cells forming short-lived and dynamic contacts with tumor cells. Furthermore, we provide evidence that distinct intensities of calcium elevation upon target recognition account for the different modes of interactions used by NK cells and CTLs during effector function.

RESULTS

Rae-1β Expression Results in Increased Intratumoral NK Cell Density and Dissemination

To visualize the course of an NKG2D-dependent antitumor response, we relied on EL4 tumor cells transduced to express Rae-1β (Diefenbach et al., 2001). EL4 cells do not express NKG2D ligands (Diefenbach et al., 2000) and were not rejected in wild-type C57BL/6 recipients upon subcutaneous injection. In contrast, EL4 Rae-1β cells were rejected before the formation of a palpable tumor (Figure 1A), even after the injection of high numbers of cells (up to 50 × 10^{6}, data not shown), thus precluding analysis of intratumoral immune responses. Because rejection of EL4 Rae-1β tumors has been shown to be NK cell-dependent on the basis of depletion studies (Diefenbach et al., 2001), we assessed their growth in lymphocyte-deficient (T, B, and NK cells) *Rag2*$^{-/-}$*Il2rg*$^{-/-}$ mice (Colucci et al., 1999). As expected, EL4 Rae-1β cells formed solid tumors in *Rag2*$^{-/-}$*Il2rg*$^{-/-}$ animals (Figure 1B), and this growth could be prevented by adoptive transfer of NK cells purified by negative selection 4 days before tumor injection (Figure 1B). In order to visualize NK cells within an established tumor, we reconstituted *Rag2*$^{-/-}$*Il2rg*$^{-/-}$ mice with 2 × 10^{6} GFP expressing NK cells 4 days after the injection of EL4 Rae-1β cells. With this approach, we observed delayed tumor growth at early time points (Figure 1B), thus providing us with a model to study the response of NK cells in the context of a solid tumor. As response through the NKG2D pathway may decrease NK cell activity over time (Coudert et al., 2005), we chose to perform experiments at the earliest time point at which the tumor could be easily visualized, i.e., 4 days after NK cell transfer.

First, we quantified NK cell infiltration in solid EL4 mCFP or EL4 Rae-1β mYFP tumors by confocal imaging of frozen tumor sections (Figures 1C and 1D). NK cell density was markedly increased in tumors expressing Rae-1β (1173 ± 189 cells/mm^{3}) compared to control tumors (301 ± 70 cells/mm^{3}) (Figure 1E).

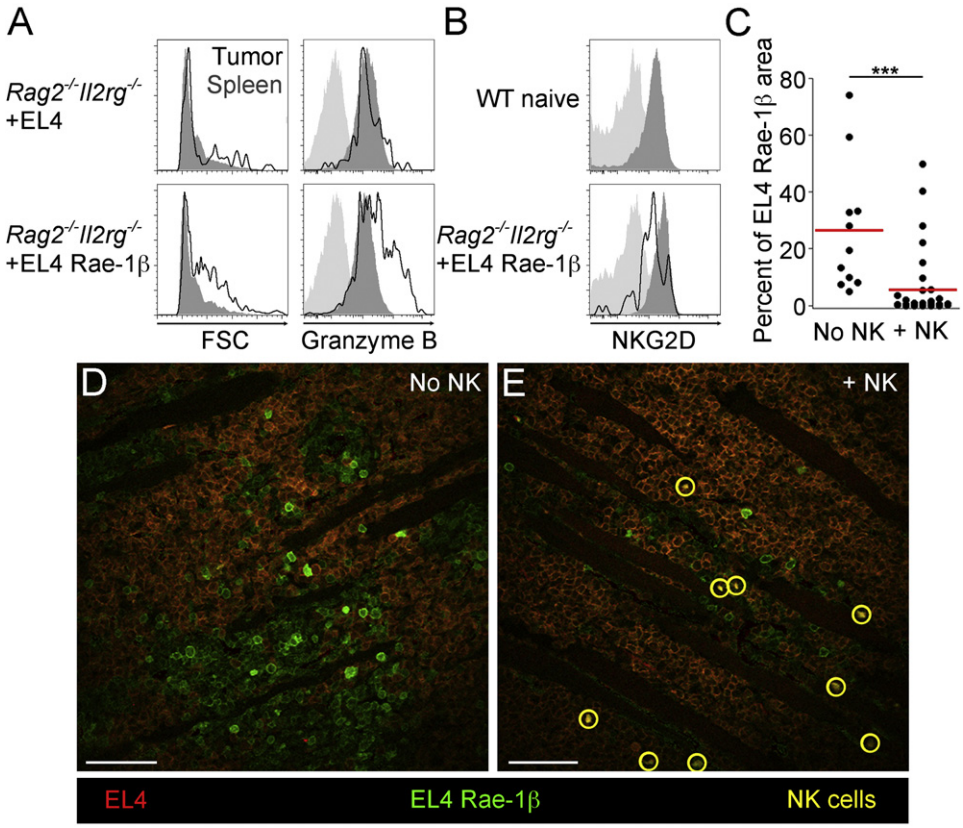

Figure 2. Infiltrating NK Cells Display Hallmarks of Activation and Specifically Eliminate EL4 Rae-1β Tumor Cells

(A) GFP expressing NK cells were adoptively transferred in *Rag2*$^{-/-}$*Il2rg*$^{-/-}$ mice bearing an EL4 (top row) or an EL4 Rae-1β (bottom row) solid tumor. Forward side scatter and intracellular granzyme B content of tumor infiltrating (black lines) and splenic NK cells (gray area) were quantified by flow cytometry 4 days after transfer. Cells were gated on live GFP$^+$ NK1.1$^+$ populations; isotype control is displayed in light gray. These results are representative of two independent experiments, with three mice per group.

(B) NKG2D expression was measured on GFP$^+$ NK1.1$^+$ NK cells in spleen and tumors of *Rag2*$^{-/-}$*Il2rg*$^{-/-}$ mice bearing an EL4 Rae-1β tumor (bottom row) or on NK cells of wild-type naive mice (top row). Intratumoral NK cells are displayed as a black line, splenic NK cells are displayed as dark-gray filled histograms, and negative controls are displayed as light-gray filled histograms.

(C) Percentage of tumor surface occupied by EL4 Rae-1β cells eight days after the injection of a mixture of mCFP expressing EL4 and mYFP expressing EL4 Rae-1β cells. Each dot corresponds to one 775 × 775 × 10 μm section ($p < 0.001$).

(D and E) Representative images of mixed EL4 (red) and EL4 Rae-1β (green) tumors in the absence (D) or presence of transferred NK cells (E, NK cells in yellow circles). Scale bars represent 100 μm.

This difference was also confirmed by flow cytometry with 338 ± 73 NK cells per million cells in EL4 tumors and 1798 ± 309 NK cells per million cells in EL4 Rae-1β tumors. Interestingly, we observed a wide range of cell densities, even within the same tumor. Staining of blood vessels revealed that most NK cells (70.0% ± 9.4%) were in direct contact with the vasculature in control EL4 tumors. In contrast, NK cells were disseminated throughout tumors expressing the NKG2D ligand, with only 29.9% ± 5.7% associated with vessels (Figure 1F). Of note, the percentages of NK cells in spleens were similar in mice bearing EL4 Rae-1β tumors and control EL4 tumors (Figure 1G). This observation strongly suggested that the higher density of NK cells in EL4 Rae-1β tumors was caused by an increased recruitment to the tumor or an enhanced survival or proliferation in situ, rather than systemic changes in the NK cell niche. Thus, this experimental model allows the study of NK cells in tumors expressing NKG2D ligands. Importantly, our data demonstrate that Rae-1β expression promotes NK cell accumulation and dissemination in the tumor.

Tumor-Infiltrating NK Cells Display Hallmarks of Activation and Cytotoxic Activity

To examine the impact of tumoral Rae-1β expression on NK cell phenotype, we analyzed splenic and intratumoral NK cells by flow cytometry 4 days after transfer. We noted that NK cells were larger in EL4 Rae-1β tumors than in control EL4 tumors, whereas the size of splenic NK cells were similar in mice bearing EL4 and EL4 Rae-1β solid tumors (Figure 2A). We also measured expression of intracellular granzyme B in splenic and tumor-infiltrating NK cells. Granzyme B expression was higher in intratumoral NK cells of mice bearing an EL4 Rae-1β solid tumor (MFI of 2226 ± 770) as compared to splenic NK cells (MFI of 1158 ± 115) or NK cells present in control EL4 tumors (MFI of 1296 ± 89) (Figure 2A). Next, we assessed NKG2D amounts

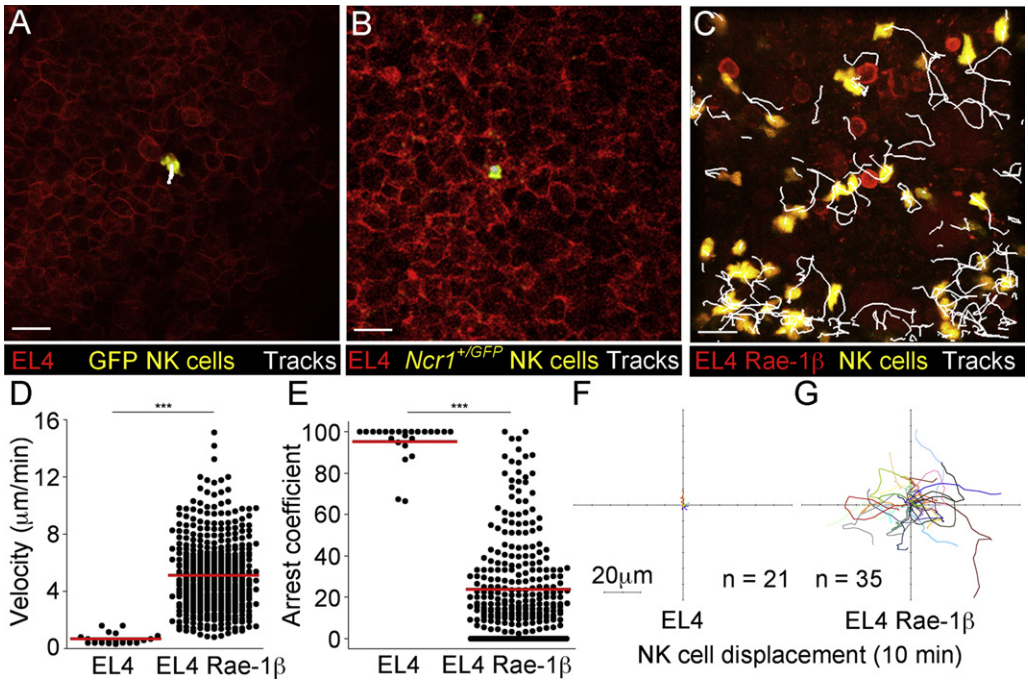

Figure 3. NK Cell Motility in EL4 and EL4 Rae-1β Tumors

(A–C) Images from two-photon movies representing transferred *UBC*-GFP NK cells (A) or endogenous *Ncr1*$^{+/GFP}$ NK cells (B) in an EL4 tumor or transferred *UBC*-GFP NK cells in an EL4 Rae-1β (C) tumor. NK cells are pseudocolored in yellow, tumor cells in red. Tracks corresponding to the displacement of NK cells during 30 min of imaging are shown in white. Scale bars represent 30 μm.

(D) Mean velocity of NK cells in EL4 and EL4 Rae-1β tumors. Each dot represents an individual NK cell.

(E) Arrest coefficient of NK cells in EL4 and EL4 Rae-1β tumors. The arrest coefficient was defined as the percentage of time a cell is moving at a velocity lower than 2 μm/min.

(F and G) Displacement of individual NK cells in EL4 (F, 21 cells) and EL4 Rae-1β (G, 35 cells) tumors; each track represents the displacement of a cell from its starting point during 10 min. Data are representative of at least four movies in three independent experiments.

and found decreased expression on intratumoral NK cells as compared to splenic NK cells, indicative of local receptor engagement (Oppenheim et al., 2005) (Figure 2B). However, expression of NKG2D was comparable on intratumoral NK cells and naive splenic NK cells from a wild-type animal (MFI of 1097 ± 198 and 930 ± 47 respectively), indicating that NKG2D was still expressed to a substantial degree. Together, these results strongly suggest that NK cells present in EL4 Rae-1β tumors are activated locally and are potentially cytotoxic. To confirm that NK cells exert cytotoxic activity on EL4 Rae-1β tumor cells, we injected a mixture of EL4 mCFP and EL4 Rae-1β mYFP tumor cells in *Rag2*$^{-/-}$*Il2rg*$^{-/-}$ mice, reconstituted half of the recipients with NK cells at day 4, and analyzed the tumor composition at day 8 by confocal microscopy. The percentage of EL4 Rae-1β tumor cells was drastically reduced in presence of NK cells (from 26.5% ± 6.8% of tumor surface in control animals to 5.5% ± 2.0% after NK cell transfer) (Figures 2C–2E), demonstrating that NK cells killed tumor cells expressing Rae-1β in a specific manner. Collectively, these data demonstrate that tumoral NKG2D ligand expression induces NK cell activation in situ, and this ultimately results in efficient and specific target cell lysis.

NK Cells Are Motile in EL4 Rae-1β but Not in EL4 Tumors

To determine whether the dissemination of NK cells in EL4 Rae-1β tumors (Figure 1F) was the result of an increase in motility in situ, we performed intravital two-photon microscopy on solid EL4 mCFP and EL4 Rae-1β mYFP tumors 4 days after the adoptive transfer of GFP-expressing NK cells. Strikingly, the motility of the few infiltrating NK cells was extremely reduced in control EL4 tumors, the mean velocity ranging from 0.3 to 1.6 μm/min (Figures 3A and 3D and Movie S1 available online). Similarly, when EL4 cells were injected in a wild-type *Ncr1*$^{+/GFP}$ mouse (Gazit et al., 2006), endogenous NK cells also displayed immotile behavior (Figure 3B and Movie S2), indicating that the transfer was not the cause of the lack of motility of NK cells in EL4 tumors. In sharp contrast, NK cells were motile when tumor cells expressed Rae-1β, with a mean velocity of 5.2 ± 0.16 μm/min (Figures 3C and 3D and Movie S3). We also quantified the arrest coefficient of NK cells in both EL4 and EL4 Rae-1β, defined as the percentage of time a cell is moving at less than 2 μm/min (Boissonnas et al., 2007). NK cells were stopped more than 95% of the time in control EL4 tumors, whereas NK cells seldom arrested when tumors expressed Rae-1β, with a mean arrest coefficient of 23.8% ± 1.4% (Figure 3E). Interestingly, NK cell velocities were strikingly similar in regions containing low or high densities of NK cells, suggesting that the increased motility is not just an enhanced freedom to move as a result of tumor cell clearance (Figure S1). In agreement with these results, the displacement of NK cells was also substantially higher in solid tumors expressing the NKG2D ligand (Figures 3F and 3G). Overall, our data indicate that the expression of Rae-1β by tumor cells

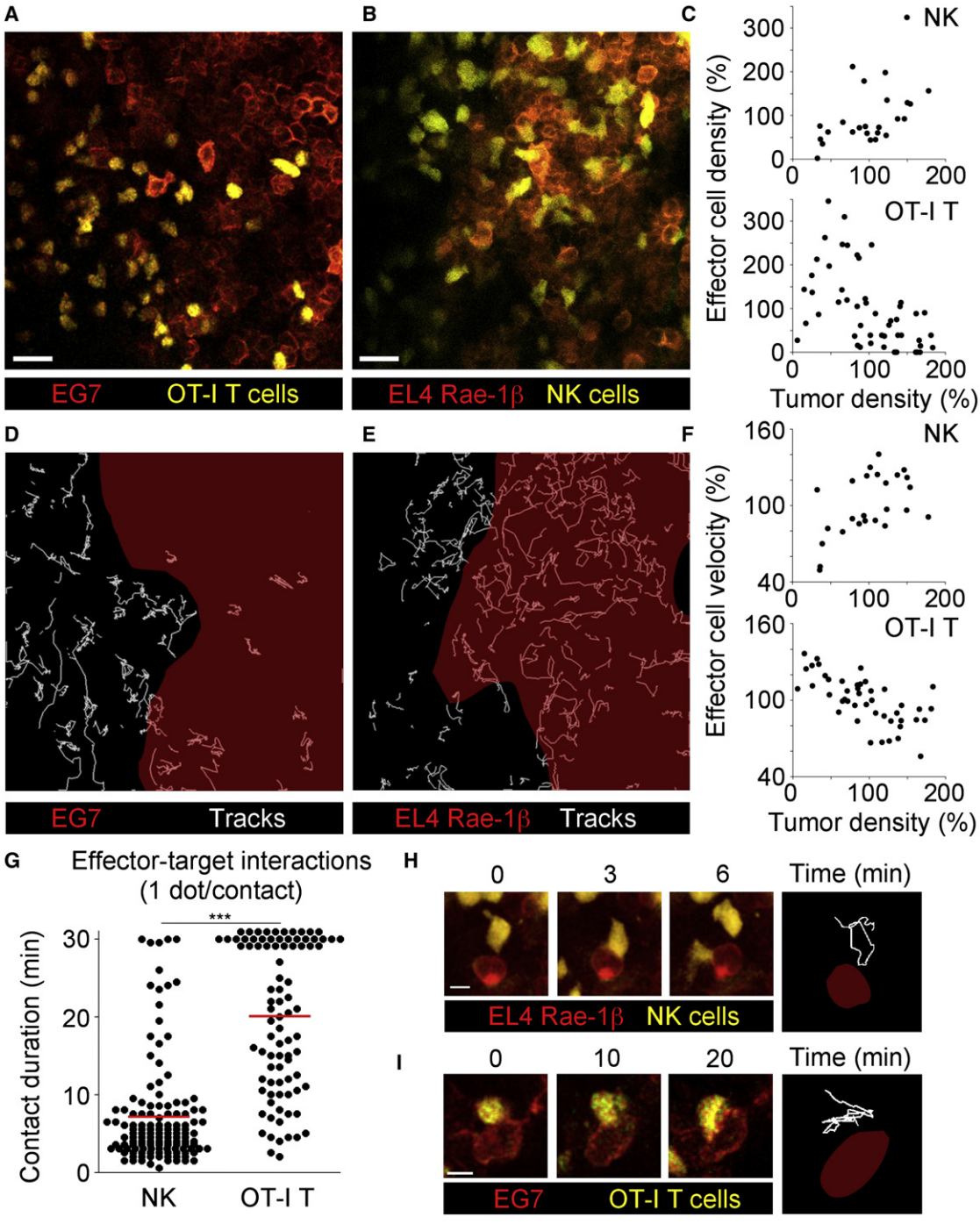

Figure 4. NK Cells but Not CD8+ T Cells Are Highly Motile in Tumor-rich Regions and Establish Short-Lasting Contacts with Their Targets

(A and B) Two-photon microscopy images representing OT-I CD8+ T cells in an EG7 mYFP tumor (A) or NK cells in an EL4 Rae-1β mYFP tumor (B). Effectors are pseudocolored in yellow; tumor cells are shown in red. Scale bars represent 25 μm.

(C) Each dot represents the mean density of NK (upper graph) or T cells (lower graph) as a function of mean tumor signal in a given region. Data are expressed as a percentage of the mean cell density of the movie.

(D and E) Schematic representation of EG7 (D) and EL4 Rae-1β (E) tumor cell-rich regions (red). Tracks representing the displacement of CTLs (D) and NK cells (E) are shown in white.

(F) Mean velocity of NK (upper graph) or T cells (lower graph) as a function of mean tumor signal. Data are expressed as a percentage of the mean effector velocity and tumor density of the movie.

(G) Contact durations between effectors and individual tumor cells. Contacts lasting for the whole movie are depicted as 30 min long (3/130 for NK cells, 35/88 for CTLs).

promotes, either directly or through changes in the microenvironment, a robust NK cell motility.

Intratumoral NK Cells Transiently Interact with Their Targets

Given that CD8$^+$ T cells and NK cells share similar mechanisms to mediate cytotoxic activity (Russell and Ley, 2003), we compared their behaviors in solid tumors. To study CTL-mediated killing, we injected EL4 tumor cells expressing ovalbumin (referred to as EG7) in *Rag2*$^{-/-}$*Il2rg*$^{-/-}$ and transferred activated CD8$^+$ T cells bearing the OT-I transgenic TCR. As previously reported (Boissonnas et al., 2007; Breart et al., 2008; Mrass et al., 2006), CTLs readily infiltrated the tumor, in which they could subsequently be visualized by intravital two-photon microscopy. To determine how tumor density influences NK and T cell behavior, we quantified the number and velocity of effectors in distinct areas of the tumor as a function of tumor cell density. CTL density was markedly reduced in tumor cell-rich areas ($p < 0.001$) and most CTLs were found in close proximity to the border of such areas (Figures 4A and 4C; Movie S4 and Table S1). In contrast, the density of NK cells appeared less dependent on tumor density, with even a small increase in NK cell numbers in tumor cell-rich regions ($p < 0.05$) (Figures 4B and 4C and Movie S5). In agreement with these results, we found decreased T cell motility in regions displaying a high tumor cell density ($p < 0.001$), whereas mean NK cell velocity was slightly increased in these regions ($p < 0.01$) (Figures 4D–4F and Table S1). Furthermore, the quantification of the contact durations between effector and tumor cells revealed that T cells mainly establish long-lasting contacts, with more than half of the interactions lasting more than 20 min. Strikingly, NK cells interacted with their targets for much shorter periods. Most NK cells indeed established contacts of either very short or intermediate durations (48.9% of contacts lasted less than 5 min, 35% of contacts lasted from 5 to 10 min) (Figures 4G–4I). To determine whether these differences in killing dynamics could be extended to other contexts, we imaged NK cell and CTL behaviors during killing of target cells (MHC-deficient and peptide-pulsed splenocytes, respectively) in lymph nodes. We also found sharp differences in the duration of the contacts between effector cells and their specific targets, with NK cells again only establishing short interactions, whereas T cells maintained prolonged contacts even with moving targets (Figure 5, Figure S2, and Movies S6 and S7). In summary, the comparison of NK and CD8$^+$ T cell behavior in two distinct microenvironements revealed a sharp difference in the stability of effector-target cell interactions. In tumors, this difference paralleled the ability of NK cells to disseminate and maintain their motility, whereas most CD8$^+$ T cells are retained in interaction with their targets at the border of tumor-rich regions.

NK Cells Form Fewer Stable Conjugates than CD8$^+$ T Cells during Effector Function

To examine the possibility that differences in signaling underlie the distinct behavior of NK and T cells, we performed in vitro conjugation experiments during which interaction conditions can be more easily controlled. First, we quantified the formation of effector-target cell conjugates by flow cytometry. After a 1 hr co-culture, NK cells formed significantly less conjugates with EL4 Rae-1β cells (12.9 ± 1.0%) than did OT-I T cells with EG7 tumor cells (44.9% ± 2.8%, $p < 0.001$). Nevertheless, NK cells still formed significantly more contacts with cells expressing Rae-1β than with controls (5.2% ± 0.6%, $p < 0.001$) (Figures 6A and 6B). Of note, we obtained similar results by using either naive or perforin-deficient NK cells (data not shown), demonstrating that the reduced NK conjugation was not due to the activation status of the NK cells nor to the rapid death of their targets. Given that these experiments measure the number of conjugates that are stable enough to be detected during this flow-based assay, our observations strongly suggest that CD8$^+$ T cells form more stable interactions with their targets than do NK cells. Thus, results obtained with this in vitro model are in agreement with the shorter durations of NK-EL4 Rae-1β contacts observed in vivo. To formally exclude that differences between tumor cells lines could account for the distinct contact stabilities, we also tested conjugation of NK and OT-I T cells to EL4 Rae-1β tumor cells loaded with the SIINFEKL peptide, which can be recognized by both cell types. In this setting, we also found strong differences in conjugation efficiency between both cell types (10.8% ± 1.3% for NK cells, 48.65% ± 2.0% for CTLs, data not shown). Thus, potential variability in the various cell lines could not account for the disparate conjugation efficiency of NK and CD8$^+$ T cells. Additionally, we performed similar experiments with a panel of transduced EG7 cell lines, expressing distinct amounts of Rae-1β. Increasing expression of this NKG2D ligand failed to rescue the low efficiency of stable conjugates formed by NK cells, ruling out the possibility that ligand levels were limiting in our experiments (Figure S2). Furthermore, clustering efficiencies showed little variation over a 1 to 6 hr time course (Figure 6C). Next, we evaluated the efficiency of NK and CD8$^+$ T cell cytotoxicity toward their respective targets. Remarkably, NK cell killing was very efficient (up to 2-fold higher than CTL-mediated killing) over this 6 hr period despite reduced clustering (Figure 6D). As reported previously in other models of NKG2D-mediated recognition (Hayakawa et al., 2002; Smyth et al., 2004), NK cell cytotoxicity was largely impaired in perforin-deficient effectors ($p < 0.001$) (Figure 6E), demonstrating that killing was dependent on perforin and granzymes, and therefore primarily mediated during effector-target interactions. Accordingly, we found that a substantial percentage of unconjugated NK cells expressed CD107a, a marker of recent degranulation (Figure 6F and Figure S3). This would be consistent with the idea that some NK cells had already performed their effector function and detached prior to conjugate assesment. To test the possibility that the expression of an inhibitory receptor for a self-MHC molecule prevented NK cell conjugation and/or degranulation, we assessed the influence of the expression of Ly49C and Ly49I receptors on NK cell responses to EL4 Rae-1β tumor cells. Interestingly, NK cell conjugation and degranulation in response to Rae1-β-expressing tumors

(H and I) Representative time-lapse images of a contact between an NK cell and an EL4 Rae-1β tumor cell (H, duration of 270 s) or a CTL and an EG7 tumor cell (I, duration of 30 min). Right-most panels represent cell trajectories (white) and tumor cell position (red) at the median time point. Scale bars represent 10 μm. Data are representative of two to four independent experiments.

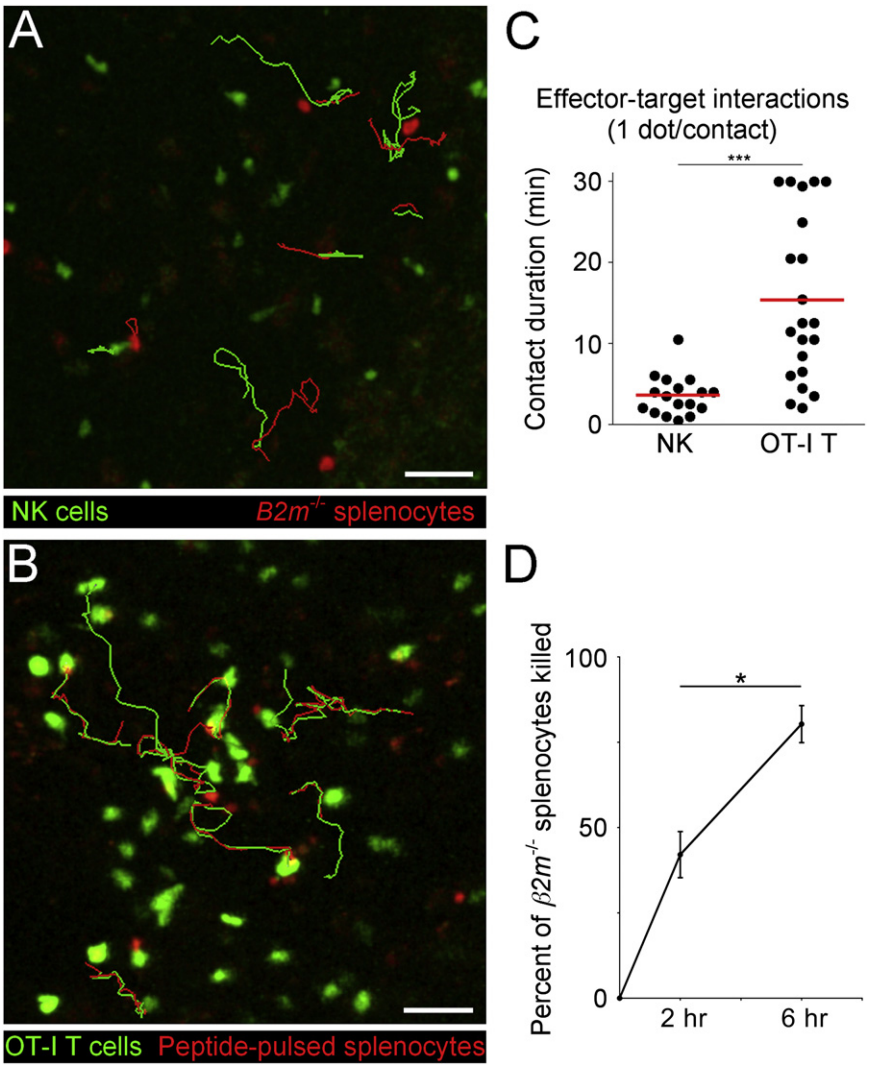

Figure 5. NK Cells Establish Short-Lasting Contacts during Elimination of MHC Class I-Deficient Cells in Lymph Nodes

(A and B) Two-photon microscopy images representing NK cells interacting with *B2m*$^{-/-}$ splenocytes (A) or OT-I T cells interacting with SIINFEKL-pulsed splenocytes (B) in intact lymph nodes. Representative trajectories (effectors in green, targets in red) are shown for cells establishing contacts. Note that OT- I T cells maintain stable contacts with moving targets (red and green tracks are superimposed) whereas NK cells only interact for a brief period (tracks are intercrossed). Scale bars represent 40 μm.

(C) Contact durations between either NK cells or CTL and their respective targets were measured from two-photon time-lapse movies ($p < 0.001$).

(D) Percentage of killed *B2m*$^{-/-}$ splenocytes was measured in vivo by flow cytometry in lymph nodes with cotransferred wild-type splenocytes as an internal control ($p = 0.029$). Data are representative of two independent experiments. Error bars represent SEM.

were relatively unaffected by expression of the inhibitory receptors Ly49C and Ly49I (Figure 6G and Figure S3). These results suggest that expression of Rae-1β largely overrides the effect of inhibition in this system. Taken together, these results demonstrate that altough NK cells are at least as efficient as CD8$^+$ T cells in eliminating targets, they form substantially less stable interactions during their killing activity.

NK Cell Conjugation Does Not Induce Sustained Calcium Flux and Is Independent of Calcium Entry

Calcium signaling is an important step in lymphocyte activation and function, and has also been associated with a stop signal for migrating T cells in tissues (Bhakta et al., 2005). Therefore, to assess whether conjugation with target cells was associated with calcium influx, we loaded effector cells with a calcium-sensitive dye, Fluo-3, and performed clustering assays after a 10 min incubation with tumor cells. This method allowed us to measure calcium concentrations simultaneously in the effectors that were or were not engaged in conjugates. As expected, the few effectors that were conjugated to control EL4 cells did not undergo calcium influx. More surprisingly, although we could observe a strong and sustained calcium elevation in T cells conjugated to EG7 tumor cells, calcium responses of NK cells conjugated to EL4 Rae-1β tumor cells were only slightly above controls (Figure 7A). Strong calcium responses were also observed in CD8$^+$ T cells interacting with peptide-pulsed EL4 Rae-1β cells, showing that the absence of calcium influx in NK cells conjugated with EL4 Rae-1β cells is not a specificity of this particular cell line. Furthermore, calcium responses in conjugated effectors appeared relatively homogeneous and we obtained similar results with two additional tumor cell lines, Bw15.02 and RMA-S, expressing distinct degrees of activating and inhibitory signals (Figure S4). These results raised the question of the contribution of calcium signaling, and in particular extracellular calcium entry, to NK cell adhesion and cytotoxicity. We thus performed killing and clustering experiments in presence of 2.5 mM EGTA to decrease the availability of extracellular calcium. Calcium chelation drastically decreased clustering between OT-I T cells and EG7 tumor cells (12.3% ± 2.3% of control, $p < 0.03$), whereas clustering between NK cells and EL4 Rae-1β tumor cells was largely unaffected (91.5% ± 6.5% of control) (Figure 7B). Of note, addition of calcium (2.5 mM $CaCl_2$) reverted clustering of T cells to control values, further confirming that decrease in free extracellular calcium was responsible for loss of CTL-EG7 conjugates, but played no substantial role during NK cell conjugation. In contrast, chelation of calcium reduced killing efficiencies of both NK and CD8$^+$ T cells close to basal amounts (8.2% ± 7.8% of control for specific killing by NK cells, 18.5 ± 7.0% for specific killing by T cells) (Figure 7C). Thus, even though elevation of intracellular calcium was limited, calcium influx appeared

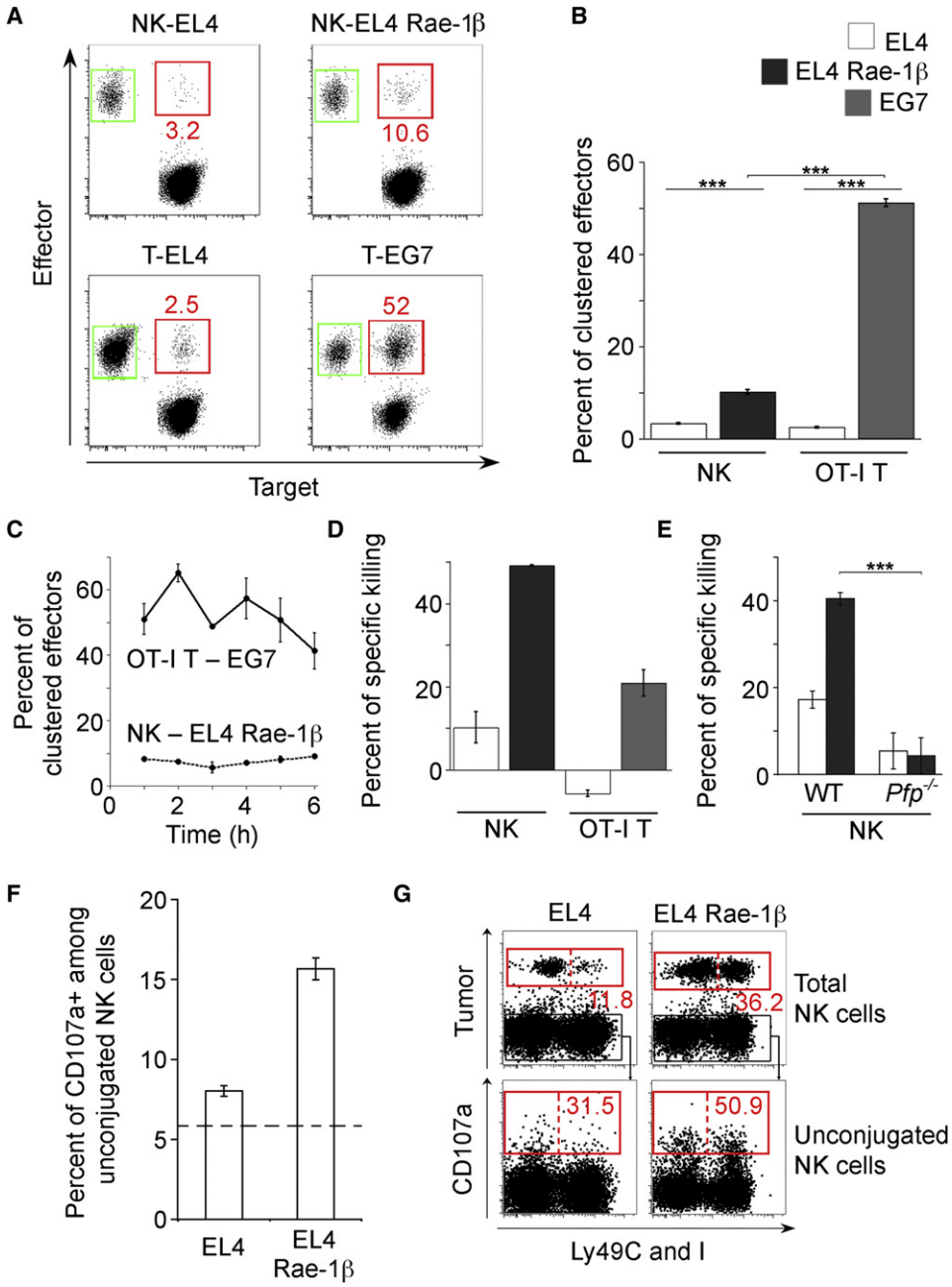

Figure 6. NK Cells Are Potent Cytotoxic Effectors Despite Reduced Adhesion to Their Targets

(A) Representative plots of conjugates between purified NK cells or OT-I T cells and tumor cells (EL4, EL4 Rae-1β, or EG7). Effectors and target cells were incubated at 37°C for 1 hr to allow conjugate formation before acquisition by flow cytometry. The percentage of effector cells engaged in a conjugate with a target cell is indicated.

(B) The percentage of clustered effector cells at 1 hr was assessed for NK cells and EL4 or EL4 Rae-1β tumor cells or OT-I T cells and EL4 or EG7 cells. Data are representative of five independent experiments that were pooled for statistical analysis ($p < 0.001$).

(C) Clustering of NK cells to EL4 Rae-1β tumor cells (dotted line) or T cells to EG7 cells (full line) for incubation periods ranging from 1 to 6 hr.

(D) Percentage of specific killing of target cells by NK or OT-I T cells at a 5:1 effector: target ratio. Data are representative of at least five experiments.

(E) Specific killing of EL4 and EL4 Rae-1β tumor cells by WT or perforin-deficient ($Pfp^{-/-}$) NK cells. Data are representative of two independent experiments.

(F) Percentage of $CD107a^+$ cells among unconjugated NK cells in presence of EL4 and EL4 Rae-1β tumor cells. The dotted line indicates the amount of background (staining on NK cells alone).

(G) As shown in the upper row, conjugation to tumor cells is analyzed as a function of Ly49C and Ly49I expression. As shown in the lower row, unconjugated NK cells were assayed for CD107a expression as a function Ly49C and Ly49I expression. Numbers indicate the percentages of Ly49C- or Ly49I-expressing cells among respectively clustered NK cells (upper row) and among unconjugated $CD107a^+$ NK cells (bottom row). Error bars represent SEM.

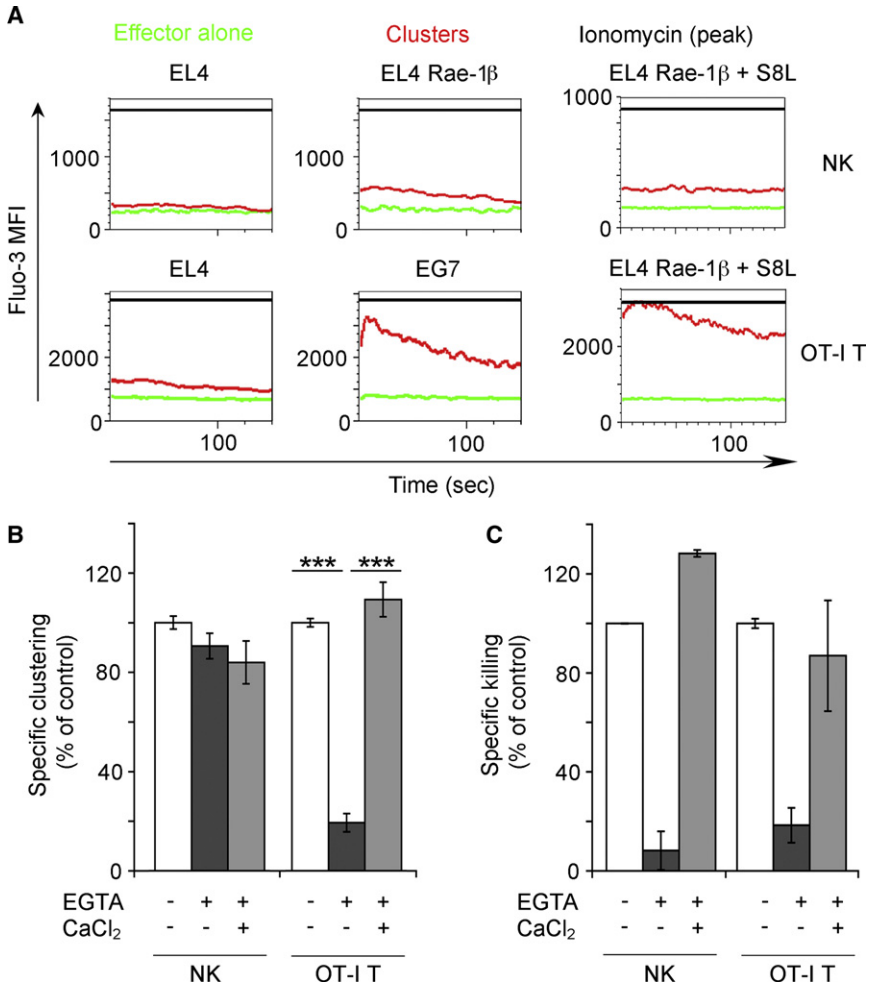

Figure 7. Distinct Intensities and Roles of Calcium Influxes during NK Cells and CTLs Interactions with Targets

(A) Effector cells were loaded with the calcium indicator Fluo-3-AM and incubated for 10 min with the indicated tumor cells (EL4, EL4 Rae-1β, EG7, or EL4 Rae-1β loaded with 10nM SIINFEKL, referred to as S8L, peptide) before analysis by flow cytometry. Mean fluorescence intensity in the Fluo-3 channel is plotted for effector cells alone (green) or effector cells participating in a conjugate (red). Black lines represent the maximum value of Fluo-3 signal in the presence of 10 μM ionomycin. Data are representative of two independent experiments.

(B and C) Percentage of specific clustering (B) and specific killing (C) in presence or absence of 2.5 mM EGTA and 2.5 mM $CaCl_2$. Values are expressed as the percentage of specific activity (e.g., for NK cells, percentage of clustering with EL4 Rae-1β minus percentage with EL4) in comparison to controls (no EGTA nor $CaCl_2$). Data are pooled from two to three independent experiments ($p < 0.001$). Error bars represent SEM.

necessary during NK cell killing. Overall, our results shed light on different patterns of calcium signaling in NK and $CD8^+$ T cells during effector function. Indeed, calcium influx appears to be a critical part in both adhesion and cytotoxicity of $CD8^+$ T cells, and robust conjugation was associated with an important and sustained elevation of intracellular calcium levels. In sharp contrast, NK cells only underwent limited or transient calcium influxes that appeared necessary for cytotoxicity but did not play a role in the low degree of adhesion to targets. Altogether, these data suggest that different patterns of calcium influxes were associated with the distinct behaviors of NK cells and CTLs during killing.

DISCUSSION

NK cell-based antitumoral therapies are the focus of intense research (Terme et al., 2008), yet the dynamics of NK cells in tumors remain poorly understood. In this study, we took advantage of the EL4 tumor model to induce subcutaneous tumors that can readily be imaged by two-photon microscopy. Additionally, a variant of this tumor expressing the NKG2D ligand Rae-1β (Diefenbach et al., 2001) was used for determining the effect of NKG2D engagement on NK cell behavior. Our results demonstrate that NK and $CD8^+$ T cells exert their effector functions with strikingly distinct dynamics and suggest an important role of calcium influx patterns in the regulation of effector-target interactions.

The demonstration that NKG2D ligand expression induces an increase in intratumoral NK cell density and dissemination extends previous findings that NK cells accumulate in the peritoneal cavity after an intraperitoneal (i.p.) injection of MHC class I-deficient (Glas et al., 2000) or Rae-1β-expressing cells (Diefenbach et al., 2001) and show that the accumulation can also take place within the microenvironment of a solid tumor. Because NK cell recruitment in tumors has been shown to be at least partly dependent on IFN-γ (Wendel et al., 2008), it is possible that activation of the first infiltrating NK cells by Rae-1β drives additional recruitment through chemokine production. Potential candidates include CXCR3 ligands CXCL 9, 10, and 11 that have been found to be induced by IFN-γ and drive NK cell mobilization (Wald et al., 2006; Wendel et al., 2008). This hypothesis would be consistent with the high variability of NK cell infiltration observed in EL4 Rae-1β tumors, given that NK cell-rich regions would hold the most potential to attract new NK cells. In addition, such an increase in local chemokine concentrations may also be responsible for the elevated NK cell motility we observed in presence of Rae-1β. Alternatively, cell-intrinsic activation of NK cells through NKG2D might directly promote their motility. Future studies comparing the homing and motility of wild-type and NKG2D deficient NK cells (Guerra et al., 2008) will allow discrimination of direct and indirect effects of NKG2D recognition.

Although CTL and NK cells induce tumor cell lysis through similar mechanisms (Russell and Ley, 2003), our results demonstrate that these two populations display drastically distinct behaviors in situ. In good agreement with previous studies

(Boissonnas et al., 2007; Breart et al., 2008; Mrass et al., 2006), we found that most tumor-specific CD8+ T cells displayed a sessile behavior during the early phase of a response and established long-lasting contacts (>20 min) during effector function. NK cells however were motile even in close proximity of tumor cells and most of them established short-lasting contacts with target cells (<10 min). Furthermore, our in vitro conjugation experiments confirmed that NK cells formed significantly less stable conjugates with their targets despite efficient cytotoxicity. The previous finding that NK cell cytoskeleton polarization may be intrinsically slow (Wülfing et al., 2003) could contribute to this phenomenon. Interestingly, when we imaged NK cell activity in a different context, namely the lysis of MHC-deficient splenocytes in lymph nodes and compare it to CTL killing of peptide-pulsed splenocytes, we detected the same differences in contact dynamics as observed in tumors. Our results extend the recent findings of Garrod et al. that have analyzed NK cell killing of allogeneic targets in lymph nodes (Garrod et al., 2010; Garrod et al., 2007). In this study, NK cell interacted for longer period of time with allogeneic than with syngeneic cells, yet most contacts lasted no more than 10 min, a duration substantially shorter than that described for CTL-target contact in vivo (Breart et al., 2008; Mempel et al., 2006). It is therefore interesting to consider that the differences of NK cell and CTL dynamics uncovered in tumors reflect a more general characteristic of their effector activity.

In vitro (Eriksson et al., 1999; Wülfing et al., 2003) and in vivo (Garrod et al., 2007) studies have indicated that the lytic hit can be delivered by NK cells in less than 10 min at least for a fraction of contacts, suggesting that the contacts lasting 5–10 min in EL4 Rae-1β tumors might be long enough to participate in cytotoxic function. However, the functional outcome of such interactions remains to be determined as we only detect physical signs of lysis, as blebbing, in few instances. Interestingly, a study of melanoma lysis showed that killing requires several lytic hits (Caramalho et al., 2009), raising the possibility of an additive effect of individual short contacts. Alternatively, target cell death might also be delayed, and thus only occur after the NK cell detachment, complicating the assessment of killing events. The ability of NK cells to establish multiple contacts over short periods could also favor the serial killing capacity that has been described in vitro (Bhat and Watzl, 2007). Although technically challenging at the moment, recording the entire contact history of target and effector cells may allow discrimination between these possibilities.

Conjugation (Burshtyn et al., 2000) and calcium signaling (Valiante et al., 1996) in NK cells result from a balance between activating and inhibiting signals. Likewise, NK cells integrate both positive and negative signals during spreading and synapse formation (Culley et al., 2009). It was therefore possible that expression of MHC class I molecules by tumor cells may have favored the transient interactions established by NK cells. When we stained conjugates for inhibitory receptors, it appeared that Ly49C and Ly49I expression did not substantially alter conjugation and degranulation in presence of Rae-1β+ tumor cells, implying that NKG2D signaling largely overrides inhibiting signals in our model. Furthermore, we did not observe an increased clustering with cells expressing higher amounts of Rae-1β or tumor cells lacking MHC I expression, suggesting that the low clustering of NK cells occurs in a number of different conditions leading to cytolysis.

To refine our analysis of the divergent behaviors of NK and CD8+ T cells, we analyzed the role of calcium signaling during contacts with target cells. Strikingly, whereas virtually all T cells engaged in conjugates displayed high intracellular calcium concentrations, NK cells showed at best a weak calcium elevation during conjugation. Of note, it has been shown that NKG2D crosslinking by antibodies induces robust calcium elevation (Jamieson et al., 2002). Our results suggest that a lower magnitude and duration of calcium elevation is induced during short-lived interactions between NK cells and their targets. Intracellular calcium influx has been shown to be associated with a stop signal for T cells (Bhakta et al., 2005), and we demonstrate here the requirement of calcium influx for CTL conjugation to tumor cells. In this respect, the weak calcium response of NK cells is a likely explanation for their reduced contact durations in vivo. This rapid disruption of contacts probably leads to the increased dissemination and motility of NK cells we observed in tumor-rich areas, whereas T cells are retained at the border of such regions by long-lasting contacts. In both cell types, killing appeared dependent on calcium availability, which is in agreement with previous studies showing calcium dependence on granule exocytosis (Pores-Fernando and Zweifach, 2009; Pores-Fernando et al., 2009). Our results thus suggest that whereas T cells undergo a sustained elevation of intracellular calcium critical to their adhesion and cytotoxicity, NK cells only undergo transient and/or limited calcium influxes, which do not induce strong adhesion but yet remain sufficient for granule exocytosis. The small amount of NK cell clustering observed in this study appears to be calcium independent as suggested by a previous report that has analyzed PLCγ2-deficient NK cells (Caraux et al., 2006).

In conclusion, this study reports the visualization of the role of NKG2D recognition on NK cell dynamics in a solid tumor. Our results shed light on drastic differences between CD8+ T cells and NK cells during effector function with respect to interactions with target cells and calcium signaling. By using distinct modes of killing and disseminating differentially in the tumor, NK cells and CTLs may act synergistically. The existence of these complementary strategies may offer new perspectives for the design of immunotherapeutical intervention.

EXPERIMENTAL PROCEDURES

Mice

C57BL/6 mice were purchased from Charles River laboratories. *Ncr1*$^{+/GFP}$ (Gazit et al., 2006), *UBC*-GFP (Jackson Laboratories), *Rag2*$^{-/-}$, *Rag2*$^{-/-}$ *Il2rg*$^{-/-}$, and OT-I TCR transgenic mice were bred in our animal facility. *Pfp*$^{-/-}$ and *B2m*$^{-/-}$ mice were a kind gift from S. Amigorena and M. Albert. All animal experiments were performed in accordance with institutional guidelines for animal care and use.

Tumor cells

EL4 and EG7 tumor cell lines were purchased from the American Type Culture Collection, EL4 Rae-1β cell line was a kind gift from D. Raulet (Diefenbach et al., 2001). Membrane-targeted CFP or YFP (mCFP or mYFP) encoding constructs were cloned in hygro pcDNA3.1 (Invitrogen). Tumor cells were transfected by electroporation, grown in complete RPMI medium (Invitrogen) containing the appropriate antibiotic and one clone was selected for each tumor line. Cells were mycoplasma-free as confirmed with Plasmotest

(Invivogen). For injections, tumor cells were harvested at late exponential phase and 5 × 10^6 cells in 50 μl of PBS were injected subcutaneously (s.c.) in the leg. Tumor volumes were monitored every 2 days with a caliper (Mitutoyo) and volumes were calculated under the assumption that tumors were half-spherical.

Cell Purification and Adoptive Transfer

NK cells were purified by negative selection from *Rag2*$^{-/-}$ *UBC*-GFP mice with the NK cell isolation kit (Miltenyi) in accordance to the manufacturer's instructions. Four days after transfer, more than 95% of GFP$^+$ cells were NK1.1$^+$ in the spleen and the tumor. For CTL generation, spleens from OT-I *UBC*-GFP mice were harvested, dissociated on a cell strainer, and activated for 4 days in complete RPMI with 25U/mL IL-2 (Roche) and 10 nM SIINFEKL (NeoMPS). More than 98% of injected cells were CD8$^+$. For adoptive transfer, 2 × 10^6 NK or CD8$^+$ T cells were injected intravenously (i.v.) into tumor-bearing mice.

Confocal imaging

Tumors were excised 4 days after NK cell injection, fixed in paraformaldehyde-lysine-periodate, dehydrated in sucrose, and snap-frozen in OCT (Sakura Finetek). Ten-micrometer-thick sections were rehydrated (six consecutive sections were collected every 100 μm throughout the entire tumor), blocked with anti-CD16/32 (clone 93, eBiosciences), and stained with biotin-anti-PECAM-1 mAb (clone ER-MP12, BMA) and then PE-conjugated streptavidin (PharMingen). Sections were then mounted in Vectashield medium (Vector Laboratories) and imaged with a confocal microscope (DM6000B, Leica Microsystems). Data were processed with the ImageJ software (NIH, version 1.40).

Flow Cytometry

Spleen and tumors from mice were collected 4 days after NK cell transfer and dissociated in RPMI containing 1 mg/mL collagenase and 0.05 mg/mL DNase (Sigma). After Fc-receptor blocking, cells were stained with PE-Cy7-conjugated anti-NK1.1 (PK136) and biotin-coupled anti-NKG2D (CX5) and then APC-conjugated streptavidin (eBiosciences). For intracellular staining, cells were fixed and permeabilized with Cytofix/Cytoperm Kit (BD Biosciences), washed, and stained with APC-conjugated anti-granzyme B (clone GB11, Invitrogen) in presence of anti-CD16/32. Acquisition was performed on a FACS Canto II cytometer (BD) and data were analyzed on FlowJo (TreeStar, version 8.8.2).

Intravital Two-Photon Imaging

Intravital tumor imaging was realized as described previously (Breart et al., 2008). In brief, anesthetized mice were placed on a custom-made heated stage and the skin above the tumor was carefully removed. The leg was immobilized with a plaster cast and a coverslip attached to a heated metal ring was set on top of the tumor to maintain the temperature at 37°C. For the visualization of NK and CTL activity in lymph nodes, GFP$^+$ endogenous NK cells were activated with polyI:C or preactivated GFP$^+$ OT-I T cells were adoptively transferred in a B6 mouse. A total of 1 × 10^7 SNARF-labeled targets (respectively *B2m*$^{-/-}$ or SIINFEKL-pulsed splenocytes) were injected after 18 hr, and imaging was performed on explanted lymph nodes 2 hr after injection. Two-photon imaging was performed on an upright microscope (DM6000B, Leica Microsystems) with a water-dipped 20×/0.95NA objective (Olympus). Sample excitation was provided by a Ti:sapphire laser (Coherent) tuned at 950 nm and emitted fluorescence was collected with four non-descanned detectors (Leica Microsystems). Typically, we recorded 5 to 10 z slices separated by 5 μm every 30 s for 30 min. Movies were then processed with the ImageJ software and analyzed with Imaris (Bitplane, version 5.7). For measuring the impact of tumor cell density on NK and T cell behavior, projections of the movies were split in 5 × 5 regions in the x and y directions. In each of these regions, we quantified the mean fluorescence intensity of tumor signal, the number of effector cells (averaged over time), and the mean instant velocity of effector cells. Contacts were defined as the absence of black pixels between two cells in at least one plane and two consecutive images. Contact durations correspond to the amount of time effector cells were seen interacting with a single target cell during a 30 min movie and thus represent a minimal estimation of the actual contact time.

Conjugation and Cytotoxicity Assays

NK cells were negatively purified from the spleens of *Ncr1*$^{+/GFP}$ mice injected 18 hr before with 250 μg of polyI:C i.p. OT-I CTLs were prepared and activated as described above. When indicated, EL4 Rae-1β tumor cells were pulsed with 10nM SIINFEKL peptide in serum-free medium for 20 min at room temperature. Effector cells were labeled with 1 μM Far Red DDAO-SE and target cells with 10 μM Cell Tracker Blue (Invitrogen). Effectors (1 × 10^5cells) and targets (4 × 10^5) were mixed in 200 μl complete RPMI, spun for 1 s at 1200 rpm, and incubated 1 hr at 37°C before conjugates were quantified by flow cytometry. For NK cells, contaminating cells were excluded from the analysis on the basis of the GFP fluorescence. For additional stainings, clusters were performed for 1 hr in presence of Alexa 647-conjugated anti-CD107a (clone 1D4B, eBiosciences). Conjugation was stopped after 1 hr with cold PBS 2% FCS. Cells were then incubated for 20 min at 4°C with PE-conjugated anti-Ly49C/I (clone 5E6, BD Biosciences) and washed before acquisition. Identical tubes without antibody or incubation at 4°C were run in parallel to control that the procedure only minimally affected conjugation efficiency. For killing experiments, effector and target cells were mixed at a 5:1 effector/target ratio in 96-well plates and spun 1 s at 1200 rpm. After 6 hr, remaining target cells were counted by flow cytometry with Caltag counting beads (Invitrogen). Cell viability was assessed with propidium iodide (Sigma). Data are presented as the percentage of specific killing, calculated as 100× (1 − target cells in well/target cells in well without effectors). Measurement of intracellular calcium concentrations was performed as described before (Beuneu et al., 2009): effectors were loaded with 5 μM Fluo-3 in RPMI + 0.2% Pluronic (Sigma) for 30 min, washed, and incubated with targets cells for 10 min before sample acquisition. When indicated, RPMI (0.424 mM free Ca^{2+}) was supplemented with 2.5 mM EGTA (final concentration of 43nM free Ca^{2+}) or 2.5 mM EGTA and 2.5 mM $CaCl_2$ (0.422 mM free Ca^{2+}) (Sigma).

Statistics

All statistical analyses were performed with a Mann-Whitney Wilcoxon unpaired test and KaleidaGraph software (Synergy software, v4.03). p values lower than 0.05 were considered significant. All data are presented as mean ± SEM.

SUPPLEMENTAL INFORMATION

Supplemental Information includes four figures, one table, and seven movies and can be found with this article online at doi:10.1016/j.immuni.2010.09.016.

ACKNOWLEDGMENTS

We thank D. Raulet for providing tumor cell lines and plasmids, E. Robey and members of the Bousso lab for helpful comments on the manuscript, and Plate-forme de Cytométrie, Institut Pasteur. We acknowledge M. Hasan and the Center for Human Immunology at Institut Pasteur for support in conducting this study. This work was supported by Institut Pasteur, INSERM, Mairie de Paris and by a Marie Curie Excellence grant. J.D., B.B., and P.B. designed the research; J.D., B.B., and F.L. performed the research; J.P.D. provided critical reagents; J.D. analyzed data; and J.D. and P.B. wrote the paper.

Received: February 22, 2010
Revised: July 2, 2010
Accepted: August 12, 2010
Published online: October 14, 2010

REFERENCES

Beuneu, H., Deguine, J., Breart, B., Mandelboim, O., Di Santo, J.P., and Bousso, P. (2009). Dynamic behavior of NK cells during activation in lymph nodes. Blood *114*, 3227–3234.

Bhakta, N.R., Oh, D.Y., and Lewis, R.S. (2005). Calcium oscillations regulate thymocyte motility during positive selection in the three-dimensional thymic environment. Nat. Immunol. *6*, 143–151.

Bhat, R., and Watzl, C. (2007). Serial killing of tumor cells by human natural killer cells—enhancement by therapeutic antibodies. PLoS ONE *2*, e326.

Boissonnas, A., Fetler, L., Zeelenberg, I.S., Hugues, S., and Amigorena, S. (2007). In vivo imaging of cytotoxic T cell infiltration and elimination of a solid tumor. J. Exp. Med. *204*, 345–356.

Breart, B., Lemaître, F., Celli, S., and Bousso, P. (2008). Two-photon imaging of intratumoral CD8+ T cell cytotoxic activity during adoptive T cell therapy in mice. J. Clin. Invest. *118*, 1390–1397.

Burgess, S.J., Maasho, K., Masilamani, M., Narayanan, S., Borrego, F., and Coligan, J.E. (2008). The NKG2D receptor: Immunobiology and clinical implications. Immunol. Res. *40*, 18–34.

Burshtyn, D.N., Shin, J., Stebbins, C., and Long, E.O. (2000). Adhesion to target cells is disrupted by the killer cell inhibitory receptor. Curr. Biol. *10*, 777–780.

Cahalan, M.D., Parker, I., Wei, S.H., and Miller, M.J. (2002). Two-photon tissue imaging: Seeing the immune system in a fresh light. Nat. Rev. Immunol. *2*, 872–880.

Caramalho, I., Faroudi, M., Padovan, E., Müller, S., and Valitutti, S. (2009). Visualizing CTL/melanoma cell interactions: Multiple hits must be delivered for tumour cell annihilation. J. Cell. Mol. Med. *13* (9B), 3834–3846.

Caraux, A., Kim, N., Bell, S.E., Zompi, S., Ranson, T., Lesjean-Pottier, S., Garcia-Ojeda, M.E., Turner, M., and Colucci, F. (2006). Phospholipase C-gamma2 is essential for NK cell cytotoxicity and innate immunity to malignant and virally infected cells. Blood *107*, 994–1002.

Cerwenka, A., Bakker, A.B.H., McClanahan, T., Wagner, J., Wu, J., Phillips, J.H., and Lanier, L.L. (2000). Retinoic acid early inducible genes define a ligand family for the activating NKG2D receptor in mice. Immunity *12*, 721–727.

Cerwenka, A., Baron, J.L., and Lanier, L.L. (2001). Ectopic expression of retinoic acid early inducible-1 gene (RAE-1) permits natural killer cell-mediated rejection of a MHC class I-bearing tumor in vivo. Proc. Natl. Acad. Sci. USA *98*, 11521–11526.

Colucci, F., Soudais, C., Rosmaraki, E., Vanes, L., Tybulewicz, V.L.J., and Di Santo, J.P. (1999). Dissecting NK cell development using a novel alymphoid mouse model: Investigating the role of the c-abl proto-oncogene in murine NK cell differentiation. J. Immunol. *162*, 2761–2765.

Coudert, J.D., Zimmer, J., Tomasello, E., Cebecauer, M., Colonna, M., Vivier, E., and Held, W. (2005). Altered NKG2D function in NK cells induced by chronic exposure to NKG2D ligand-expressing tumor cells. Blood *106*, 1711–1717.

Culley, F.J., Johnson, M., Evans, J.H., Kumar, S., Crilly, R., Casasbuenas, J., Schnyder, T., Mehrabi, M., Deonarain, M.P., Ushakov, D.S., et al. (2009). Natural killer cell signal integration balances synapse symmetry and migration. PLoS Biol. *7*, e1000159.

Diefenbach, A., Jamieson, A.M., Liu, S.D., Shastri, N., and Raulet, D.H. (2000). Ligands for the murine NKG2D receptor: Expression by tumor cells and activation of NK cells and macrophages. Nat. Immunol. *1*, 119–126.

Diefenbach, A., Jensen, E.R., Jamieson, A.M., and Raulet, D.H. (2001). Rae1 and H60 ligands of the NKG2D receptor stimulate tumour immunity. Nature *413*, 165–171.

Dunn, G.P., Old, L.J., and Schreiber, R.D. (2004). The three Es of cancer immunoediting. Annu. Rev. Immunol. *22*, 329–360.

Eriksson, M., Leitz, G., Fällman, E., Axner, O., Ryan, J.C., Nakamura, M.C., and Sentman, C.L. (1999). Inhibitory receptors alter natural killer cell interactions with target cells yet allow simultaneous killing of susceptible targets. J. Exp. Med. *190*, 1005–1012.

Garrod, K.R., Wei, S.H., Parker, I., and Cahalan, M.D. (2007). Natural killer cells actively patrol peripheral lymph nodes forming stable conjugates to eliminate MHC-mismatched targets. Proc. Natl. Acad. Sci. USA *104*, 12081–12086.

Garrod, K.R., Liu, F.-C., Forrest, L.E., Parker, I., Kang, S.-M., and Cahalan, M.D. (2010). NK cell patrolling and elimination of donor-derived dendritic cells favor indirect alloreactivity. J. Immunol. *184*, 2329–2336.

Gasser, S., Orsulic, S., Brown, E.J., and Raulet, D.H. (2005). The DNA damage pathway regulates innate immune system ligands of the NKG2D receptor. Nature *436*, 1186–1190.

Gazit, R., Gruda, R., Elboim, M., Arnon, T.I., Katz, G., Achdout, H., Hanna, J., Qimron, U., Landau, G., Greenbaum, E., et al. (2006). Lethal influenza infection in the absence of the natural killer cell receptor gene Ncr1. Nat. Immunol. *7*, 517–523.

Glas, R., Franksson, L., Une, C., Eloranta, M.-L., Ohlén, C., Orn, A., and Kärre, K. (2000). Recruitment and activation of natural killer (NK) cells in vivo determined by the target cell phenotype. An adaptive component of NK cell-mediated responses. J. Exp. Med. *191*, 129–138.

Groh, V., Rhinehart, R., Secrist, H., Bauer, S., Grabstein, K.H., and Spies, T. (1999). Broad tumor-associated expression and recognition by tumor-derived gamma delta T cells of MICA and MICB. Proc. Natl. Acad. Sci. USA *96*, 6879–6884.

Guerra, N., Tan, Y.X., Joncker, N.T., Choy, A., Gallardo, F., Xiong, N., Knoblaugh, S., Cado, D., Greenberg, N.M., Greenberg, N.R., and Raulet, D.H. (2008). NKG2D-deficient mice are defective in tumor surveillance in models of spontaneous malignancy. Immunity *28*, 571–580.

Hayakawa, Y., Kelly, J.M., Westwood, J.A., Darcy, P.K., Diefenbach, A., Raulet, D., and Smyth, M.J. (2002). Cutting edge: Tumor rejection mediated by NKG2D receptor-ligand interaction is dependent upon perforin. J. Immunol. *169*, 5377–5381.

Jamieson, A.M., Diefenbach, A., McMahon, C.W., Xiong, N., Carlyle, J.R., and Raulet, D.H. (2002). The role of the NKG2D immunoreceptor in immune cell activation and natural killing. Immunity *17*, 19–29.

Lanier, L.L. (2005). NK cell recognition. Annu. Rev. Immunol. *23*, 225–274.

Mempel, T.R., Pittet, M.J., Khazaie, K., Weninger, W., Weissleder, R., von Boehmer, H., and von Andrian, U.H. (2006). Regulatory T cells reversibly suppress cytotoxic T cell function independent of effector differentiation. Immunity *25*, 129–141.

Mrass, P., Takano, H., Ng, L.G., Daxini, S., Lasaro, M.O., Iparraguirre, A., Cavanagh, L.L., von Andrian, U.H., Ertl, H.C.J., Haydon, P.G., and Weninger, W. (2006). Random migration precedes stable target cell interactions of tumor-infiltrating T cells. J. Exp. Med. *203*, 2749–2761.

Nausch, N., and Cerwenka, A. (2008). NKG2D ligands in tumor immunity. Oncogene *27*, 5944–5958.

Oppenheim, D.E., Roberts, S.J., Clarke, S.L., Filler, R., Lewis, J.M., Tigelaar, R.E., Girardi, M., and Hayday, A.C. (2005). Sustained localized expression of ligand for the activating NKG2D receptor impairs natural cytotoxicity in vivo and reduces tumor immunosurveillance. Nat. Immunol. *6*, 928–937.

Orange, J.S. (2008). Formation and function of the lytic NK-cell immunological synapse. Nat. Rev. Immunol. *8*, 713–725.

Pores-Fernando, A.T., and Zweifach, A. (2009). Calcium influx and signaling in cytotoxic T-lymphocyte lytic granule exocytosis. Immunol. Rev. *231*, 160–173.

Pores-Fernando, A.T., Gaur, S., Doyon, M.Y., and Zweifach, A. (2009). Calcineurin-dependent lytic granule exocytosis in NK-92 natural killer cells. Cell. Immunol. *254*, 105–109.

Raulet, D.H. (2003). Roles of the NKG2D immunoreceptor and its ligands. Nat. Rev. Immunol. *3*, 781–790.

Routes, J.M., Ryan, S., Morris, K., Takaki, R., Cerwenka, A., and Lanier, L.L. (2005). Adenovirus serotype 5 E1A sensitizes tumor cells to NKG2D-dependent NK cell lysis and tumor rejection. J. Exp. Med. *202*, 1477–1482.

Russell, J.H., and Ley, T.J. (2003). Lymphocyte-mediated cytotoxicity. Annu. Rev. Immunol. *20*, 323–370.

Smyth, M.J., Swann, J., Kelly, J.M., Cretney, E., Yokoyama, W.M., Diefenbach, A., Sayers, T.J., and Hayakawa, Y. (2004). NKG2D recognition and perforin effector function mediate effective cytokine immunotherapy of cancer. J. Exp. Med. *200*, 1325–1335.

Smyth, M.J., Swann, J., Cretney, E., Zerafa, N., Yokoyama, W.M., and Hayakawa, Y. (2005). NKG2D function protects the host from tumor initiation. J. Exp. Med. *202*, 583–588.

Terme, M., Ullrich, E., Delahaye, N.F., Chaput, N., and Zitvogel, L. (2008). Natural killer cell-directed therapies: Moving from unexpected results to successful strategies. Nat. Immunol. *9*, 486–494.

Valiante, N.M., Phillips, J.H., Lanier, L.L., and Parham, P. (1996). Killer cell inhibitory receptor recognition of human leukocyte antigen (HLA) class I blocks formation of a pp36/PLC-gamma signaling complex in human natural killer (NK) cells. J. Exp. Med. *184*, 2243–2250.

Wald, O., Weiss, I.D., Wald, H., Shoham, H., Bar-Shavit, Y., Beider, K., Galun, E., Weiss, L., Flaishon, L., Shachar, I., et al. (2006). IFN-gamma acts on T cells to induce NK cell mobilization and accumulation in target organs. J. Immunol. *176*, 4716–4729.

Wendel, M., Galani, I.E., Suri-Payer, E., and Cerwenka, A. (2008). Natural killer cell accumulation in tumors is dependent on IFN-gamma and CXCR3 ligands. Cancer Res. *68*, 8437–8445.

Wülfing, C., Purtic, B., Klem, J., and Schatzle, J.D. (2003). Stepwise cytoskeletal polarization as a series of checkpoints in innate but not adaptive cytolytic killing. Proc. Natl. Acad. Sci. USA *100*, 7767–7772.

Yokoyama, W.M., Kim, S., and French, A.R. (2004). The dynamic life of natural killer cells. Annu. Rev. Immunol. *22*, 405–429.